TECHNISCHE MECHANIK, Band 16, Heft 1, (1996), 51-62
Manuskripteingang: 19. Dezember 1995

Simulation of Polycrystals Using an FEM-based Representative Volume Element

Dedicated to Erwin Stein on the event of his 65th birthday

M. Kraska, A. Bertram

The aim to predict the macroscopic behaviour of materials with microstructure on the basis of their local properties (homogenization) has led to a broad variety of methods. Here we discuss a technique called the representative volume element (RVE). This volume element, small enough to be macroscopically considered as a material point, and large enough to smoothen local inhomogeneities, is cut out of the macroscopic body and subjected to simulated loading or deformation histories. We discuss some aspects of the FEM implementation of the RVE. Special attention is paid to the influence of boundary conditions. The identification of different mechanisms leading to induced anisotropy in polycrystalline metals is demonstrated by a simple computational example.

1 Introduction

The behaviour of polycrystalline metals undergoing large inelastic deformations is a field of special interest for material scientists. Many metal forming technologies lead to large inelastic deformations (forging, rolling, deep drawing). Experience shows, that such processes are accompanied by the evolution of elastic and inelastic anisotropy in initially isotropic media. The monocrystalline grains undergo considerable changes in shape and lattice orientation, resulting in a deformation texture in the polycrystalline material. For the appropriate design of metal forming processes and estimates of the resulting properties of the material, a material model is required. This model has to be general in the sense that it covers all possible processes the material may undergo. Therefore, it is necessary to take into account the basic physical mechanisms involved, and identify their dynamics.

Our objective is to simulate the behaviour of polycrytalline aggregates based on a crystal plasticity theory for the grains which form the aggregate. The study of such simulations results in a deeper understanding of the physical behaviour of polycrystalline solids undergiong large deformations. There are several classical approaches to this problem, which have the common principal disadvantage of not being able to consider the local grain interactions. The method we want to use is based on a finite element model of a so-called representative volume element (RVE). This model enables us to consider the local crystalline structure. The question is, how much detail must be included in the structure model. For example, grain boundary mechanisms could be considered, but have been disregarded in the present paper. In fact, we limit ourselves to the local single crystal constitutive model and its connection with the global stress-strain relation. Then we consider some aspects of the finite element implementation, and finally illustrate the application of this implementation in the context of a simple example.

2 Description of Finite Inelastic Deformations

As we want to describe material behaviour at large strains, we have to ensure the objectivity of our constitutive relations. This is achieved identically by use of stress and strain measures invariant under a change of reference frame or rigid body motions. These measures are defined within the intrinsic concept of continuous bodies suggested by Noll (1972), and used extensively by Krawietz (1986), and Bertram (1989). The main idea is to consider the material body as a differentiable manifold $\mathcal{B}$ of material points P, which is mapped by the global placement κ into Euclidean point space (observer frame) $\mathcal{E}$.

$$\begin{aligned} \kappa &: \mathcal{B} \to \mathcal{E} \\ P &\mapsto \kappa(P) \end{aligned} \tag{1}$$

The differential of this mapping at a point P is $\mathbf{K}_P := \mathrm{d}\kappa(P)$, a linear mapping from the tangent space $\mathcal{T}_P\mathcal{B}$ to $\mathcal{B}$ at P into the Euclidean vector space $\mathcal{V}$ (tangent to $\mathcal{E}$):

$$\mathbf{K}_P : \mathcal{T}_P\mathcal{B} \to \mathcal{V} \tag{2}$$

Let $\mathbf{g} : \mathcal{V} \to \mathcal{V}^*$ be the Euclidean metric of $\mathcal{V}$, being symmetric and positive definite. An asterisk denotes duality of linear spaces or mappings. This metric $\mathbf{g}$ can be pulled back to the tangent space $\mathcal{T}_P\mathcal{B}$ by $\mathbf{K}_P$:

$$\mathbf{K}_P^* \, \mathbf{g} \, \mathbf{K}_P =: \mathbf{G}_P = \mathbf{G}_P^* : \mathcal{T}_P\mathcal{B} \to \mathcal{T}_P^*\mathcal{B}. \tag{3}$$

$\mathbf{G}_P$ is a metric on $\mathcal{T}_P\mathcal{B}$ and is called the *local configuration.* In the following, the index P for the material point is omitted for brevity. For materials with some special undistorted (stressfree) configuration $\mathbf{G}_u$ it is reasonable to define the intrinsic strain tensor

$$\mathbf{E}^I : \mathcal{T}_P\mathcal{B} \to \mathcal{T}_P^*\mathcal{B}, \quad \mathbf{E}^I := \frac{1}{2}\mathbf{G}_u^{-1}(\mathbf{G} - \mathbf{G}_u) \tag{4}$$

If we choose an undistorted placement $\mathbf{K}_u$ with $\mathbf{K}_u^* \, \mathbf{g} \, \mathbf{K}_u = \mathbf{G}_u$, this is obviously determined only up to arbitrary rotations. The change of placement

$$\mathbf{F} := \mathbf{K} \, \mathbf{K}_u^{-1} \tag{5}$$

is the *deformation gradient.* $\mathbf{F}$ can be used to define the Eulerian and Lagrangean strain measures $\mathbf{E}^E$ (Almansi strain tensor) and $\mathbf{E}^L$ (Green strain tensor).

$$\begin{aligned} \mathbf{E}^E &:= \frac{1}{2}(\mathbf{g} - (\mathbf{F}^{-1})^* \mathbf{g} \, \mathbf{F}^{-1}) = \frac{1}{2}(\mathbf{g} - (\mathbf{K}^{-1})^* \mathbf{G}_u \, \mathbf{K}^{-1}) \\ \mathbf{E}^L &:= \frac{1}{2}(\mathbf{F}^* \, \mathbf{g} \, \mathbf{F} - \mathbf{g}) = \frac{1}{2}((\mathbf{K}_u^{-1})^* \mathbf{G} \, \mathbf{K}_u^{-1} - \mathbf{g}) \end{aligned} \tag{6}$$

If $\mathbf{Q} : \mathcal{E} \to \hat{\mathcal{E}}$ is an (isometric) change of observer frame ($\mathbf{Q}^* \, \mathbf{g} \, \mathbf{Q} = \mathbf{g}$), then the following transformation of $\mathbf{K}$ results:

$$\hat{\mathbf{K}} = \mathbf{Q} \, \mathbf{K} \tag{7}$$

The transformation of the Cauchy stress tensor $\mathbf{T}$ under change of observer is given by

$$\hat{\mathbf{T}} = \mathbf{Q}\mathbf{T}\mathbf{Q}^* \tag{8}$$

By also pulling $\mathbf{T}$ back by $\mathbf{K}$, we define the *intrinsic stress tensor*

$$\mathbf{S} := \mathbf{K}^{-1}\mathbf{T}(\mathbf{K}^{-1})^* \tag{9}$$

which turns out to be invariant under change of observer.

Corresponding to the principle of determinism, we consider the stresses to be uniquely determined by the local values of strains, their time derivatives and a vector of internal state variables $\boldsymbol{\alpha}$.

$$\mathbf{S} = f(\mathbf{G}, \dot{\mathbf{G}}, \boldsymbol{\alpha}) \tag{10}$$

If the material point is elastic, this reduces to

$$\mathbf{S} = h(\mathbf{G}) \tag{11}$$

An elastic body is called uniform if for any points P and Q there exists a *material isomorphism* (invertible linear mapping) $\mathbf{H}_{PQ} : \mathcal{T}_P\mathcal{B} \to \mathcal{T}_Q\mathcal{B}$, such that for the elastic laws $h_P(\mathbf{G})$ and $h_Q(\mathbf{G})$ holds.

$$h_Q(\bullet) = \mathbf{H}_{PQ} \, h_P(\mathbf{H}_{PQ}^* \bullet \mathbf{H}_{PQ}) \, \mathbf{H}_{PQ}^*. \tag{12}$$

The points are then said to consist of the *same elastic material.*

A *symmetry transformation* of h_P is simply an automorphism $\mathbf{H}_P := \mathbf{H}_{PP}$, which results from setting $Q \equiv P$.

$$h_P(\bullet) = \mathbf{H}_P \, h_P(\mathbf{H}_P^* \bullet \mathbf{H}_P) \, \mathbf{H}_P^* \tag{13}$$

All such symmetry transformations form the *symmetry group* $\mathcal{G}$ of the elastic law h_P.

Applying the concept of *materials with isomorphic elastic ranges* (Bertram 1992), the material response is characterized by the following assumptions:

1. *Existence of elastic ranges.* At any instant the configuration $\mathbf{G}$ lies within some elastic range e_j, which is a subset of the total configuration space. That means that the stresses $\mathbf{S}$ are determined by the current elastic law h_j

$$\mathbf{S} = h_j(\mathbf{G}), \tag{14}$$

as long as the configuration does not leave the range e_j.

2. *Isomorphy of the elastic ranges.* The constitutive laws h_j of different elastic ranges are mutually isomorphic. If we arbitrarily choose one as a reference law h_R, this means, that for any other elastic range with elastic law h_j there is an isomorphism $\mathbf{P}_j : \mathcal{T}_P\mathcal{B} \to \mathcal{T}_P\mathcal{B}$ such that the following *condition of isomorphy* holds:

$$h_j(\bullet) = \mathbf{P}_j\, h_R(\mathbf{P}_j^* \bullet \mathbf{P}_j)\, \mathbf{P}_j^* \tag{15}$$

within the intersection of their domains.

Equation (15) leads to a natural distinction between elastic and inelastic processes. A process is called *elastic* if $\mathbf{P}$ is constant and *inelastic* if $\mathbf{P}$ changes with time. $\mathbf{P}$ is called *inelastic transformation.* A description of inelastic deformations requires the specification of a yield criterion (limits of the elastic ranges) and a flow rule, which is assumed to have the form

$$\dot{\mathbf{P}} = a(\mathbf{G}, \dot{\mathbf{G}}, \mathbf{P}, \boldsymbol{\alpha}). \tag{16}$$

A decomposition of the deformation into elastic and inelastic domains is not needed in this theory.

3 Constitutive Law for Single Crystals

A basic assumption of the present work is that the grains of a polycrystalline metal are single crystals whose constitutive response is not directly affected by the embedding into the polycrystalline aggregate, e.g. by grain shape or size.

Single crystals in general display an anisotropic elastic material response due to the regular arangement of their atoms. The regular array is called lattice. The local lattice geometry may be represented by three independent (in general non-constant) material lattice vectors $\mathbf{t}_{ti} \in \mathcal{T}_P\mathcal{B}$, oriented along the lattice axes. Their current length indicates the corresponding atom spacing (Krawietz 1986, p.190). They are accessible for measurements by X-ray diffraction or resonance tests (Han, 1995).

Elastic Law. The lattice vectors appear in the current elastic law h_t as directors of the elastic anisotropy. It is generally accepted to use linear elastic laws for metals. As long as the elastic deformations are small, the possible choices of strain and stress measure in the linear elastic law are equivalent. Thus, we choose the intrinsic *linear elastic law*

$$\mathbf{S} = h_t(\mathbf{G}) = \mathbb{C}_t[\mathbf{G} - \mathbf{G}_u], \tag{17}$$

where $\mathbb{C}_t$ is the current fourth order elasticity tensor. For a face centered cubic (f.c.c.) crystal it has the natural form

$$\mathbb{C}_t = C_t^{ijkl}\mathbf{t}_{ti} \otimes \mathbf{t}_{tj} \otimes \mathbf{t}_{tk} \otimes \mathbf{t}_{tl} \tag{18}$$

with the current lattice vectors $\mathbf{t}_{ti}$, and $\otimes$ denoting the tensor product. The reference law analogously is

$$h_R(\mathbf{G}_R) = \mathbb{C}_R[\mathbf{G}_R - \mathbf{G}_{Ru}] \quad \text{with} \quad \mathbb{C}_R = C_R^{ijkl}\mathbf{t}_{Ri} \otimes \mathbf{t}_{Rj} \otimes \mathbf{t}_{Rk} \otimes \mathbf{t}_{Rl} \tag{19}$$

Applying the condition (15) of isomorphy to equations (17), (18) and (19), we obtain the transformation of the lattice vectors and the components of the elasticity tensor under inelastic deformations.

$$\begin{aligned} \mathbf{t}_{ti} &= \mathbf{P}(\mathbf{t}_{Ri}) \\ C_t^{ijkl} &= C_R^{ijkl} \end{aligned} \tag{20}$$

Inelastic Law. In the 1920's, Taylor, Elam, Schmid, and others developed an approach of modelling the inelastic deformations in single crystals by shear in slip systems. Such a slip system consists of a slip plane

(indicated by its normal $\mathbf{n}^\alpha \in \mathcal{T}_P^*\mathcal{B}$) and a slip direction $\mathbf{d}_\alpha \in \mathcal{T}_P\mathcal{B}$. These (co-)vectors have constant representations as linear combinations of the current lattice vectors $\mathbf{t}_{ti}$ and their duals. Slip can be considered as flow of material points relative to the lattice, thereby changing the inelastic transformation $\mathbf{P}$. For one active slip system α (single slip) with slip rate $\dot{\mu}_\alpha$ the corresponding rate of $\mathbf{P}$ is given by the flow rule

$$\dot{\mathbf{P}}\,\mathbf{P}^{-1} = -\dot{\mu}_\alpha \mathbf{d}_\alpha \otimes \mathbf{n}^\alpha \tag{21}$$

For multiple slip, this equation is summed over α. The slip rates $\dot{\mu}_\alpha$ depend on the component in slip direction of the stress vector in the slip plane. This component is called *resolved shear stress* (Schmid stress) τ_α, and can be calculated as

$$\tau_\alpha = \mathrm{tr}\,(\mathbf{S}\,\mathbf{G}\,\mathbf{d}_\alpha \otimes \mathbf{n}^\alpha) \tag{22}$$

Following the Schmid law, flow occures when the resolved shear stress reaches some limit, the critical resolved shear stress (critical SCHMID stress) τ_c. The slip rate then is determined by a one-dimensional inelastic law.

$$\dot{\mu}_\alpha = f(\tau_\alpha) \tag{23}$$

For the computational example in the present work, we choose a rate-dependent law with the slip rate being proportional to the overstress.

$$\dot{\mu}_\alpha = \frac{1}{\eta}\mathrm{sg}(\tau_\alpha)\,|\,\tau_\alpha - \tau_{c\alpha}\,| \tag{24}$$

Combined with the lattice elasticity, this results in a constitutive response of the Bingham type.

The critical shear stresses $\tau_{c\alpha}$ are initially considered to be equal for each class of slip systems. Depending on the adopted hardening model, the critical shear stresses can be affected by the slip in their slip system (selfhardening) or in the other slip systems (latent hardening). For further details, see e.g. Asaro (1983), or Havner (1992).

It is evident from pure kinematical considerations that single slip in tensile specimens leads to a rotation of the lattice with respect to the load axis (see e.g. Asaro, 1983, p.9). This effect of lattice rotation is essential for the development of deformation textures and therefore has to be accounted for in simulations of finite inelastic deformations of crystalline solids.

4 Representative Volume Element

Classical Approaches. As we want to calculate the phenomenological macro-behaviour of polycrystalline solids from a given behaviour of the single crystalline grains, we have to average the local strains and stresses. This process is called homogenization. There are mainly three classical approaches corresponding to different kinematic or dynamic assumptions.

- *Taylor theory.* The local strain field is assumed to be constant in space and, thus, equal to the global strain. Each grain is uniformly deformed. The global stress is obtained by averaging over all grains. Compatibility of the aggregate is identically preserved, but in general intergranular equilibrium is violated.
- *Sachs theory.* This is the counterpart to Taylor's theory. The local stress field is assumed to be constant in space and equal to the global stress tensor. Again, each grain is supposed to deform uniformly. Global strain results from averaging over the grains. Thus, the equilibrium condition is identically fulfilled, but compatibility between grains is generally not guaranteed.
- *Self consistent schemes.* Each grain is considered to be separately embedded into a homogeneous equivalent medium (HEM). The stress and strain fields far from the inclusion are homogeneous and their values are taken as the global ones. Deformation and stress of each grain are obtained by solution of a separate boundary value problem. The constants of the phenomenological constitutive law for the HEM are iterated until the HEM behaves like the average of the grains. Thus, an inverse problem has to be solved. Compatibility and equilibrium condition are fulfilled only between single grains and the surrounding HEM.

The disadvantage of these approaches is their inability to account for the local texture of the material. They consider only the distribution of some properties, e.g., lattice orientation, over the material volume. They cannot take into account effects resulting from local interaction of neighbouring grains. This is the motivation for the representative volume element (RVE) concept, which will be described next.

First, we cut a small volume (RVE) out of the body. For this volume, a boundary value problem is formulated and solved using finite elements. It is subjected to different deformation processes in order to obtain a global load response. The RVE has to be large enough to be really representative for the macroscopically uniform material of the body. Particularly, the response of the RVE should be insensitive to small variations of its boundary position, i.e. whether the next grain is still included or not. On the other hand, the complexity is restricted by the available computational facilities.

There are basically two ways to employ the RVE. The simulation may be embedded into a macroscopic finite element analysis, serving as a numerical constitutive model on integration point level (see e.g. Schröder and Miehe, 1994). Alternatively, the RVE is subjected to the computational simulation of experiments in order to determine its material response, i.e. to identify the form of the phenomenological constitutive law.

Homogenization Procedure. Our aim is to obtain a relation between the local and global stresses $\mathbf{T}$ and $\tilde{\mathbf{T}}$ respectively, and between the local deformation field $\mathbf{F}(P)$ and the global deformation $\tilde{\mathbf{F}}$. By choice of some reference point $O \in \mathcal{E}$, we define the position vectors $\mathbf{x}$ and $\mathbf{X}$ of a material point $P \in \mathcal{B}$.

$$\begin{aligned} \mathbf{x}(P) &= \overrightarrow{O\kappa(P)} \in \mathcal{V} \\ \mathbf{X}(P) &= \overrightarrow{O\kappa_0(P)} \in \mathcal{V} \end{aligned} \tag{25}$$

Then we consider the global displacement field of the RVE $\mathbf{u}(P) := \overrightarrow{\kappa_0(P)\kappa(P)} = \mathbf{x}(P) - \mathbf{X}(P)$ (with the material at κ_0 in an undistorted state for all $P \in \mathcal{B}$). The basic idea is to split $\mathbf{u}(P) \in \mathcal{V}$ into a part $\tilde{\mathbf{F}}\,\mathbf{X}(P)$, corresponding to a homogeneous global deformation, and a local fluctuation part $\mathbf{w}(P)$.

$$\mathbf{u}(P) = \tilde{\mathbf{F}}\,\mathbf{X}(P) + \mathbf{w}(P) \tag{26}$$

The Taylor model is contained in the present model by setting $\mathbf{w}(P) = \mathbf{0}\ \forall P \in \mathcal{B}$. Assuming the displacement fluctuation $\mathbf{w}$ to vanish or being periodic on the boundary of the RVE, the global deformation gradient $\tilde{\mathbf{F}}$ can be shown to equal the mean value of the local deformation gradient $\mathbf{F} = \mathrm{d}\kappa/\mathrm{d}\kappa_0$, taken over the volume in κ_0.

$$\tilde{\mathbf{F}} = \frac{1}{V_0} \int_{\kappa_0(\mathcal{B})} \mathbf{F}(P) \mathrm{d}V_0 \tag{27}$$

(see Krawietz 1986, p. 363). A similar expression can be found for the Cauchy stress. Here the integral has to be taken over the volume in κ (actual placement).

$$\tilde{\mathbf{T}} = \frac{1}{V} \int_{\kappa(\mathcal{B})} \mathbf{T}(\kappa) \mathrm{d}V \tag{28}$$

Homogeneous Boundary Conditions. Let the condition of vanishing boundary displacement fluctuations be called *homogeneous boundary conditions*. In this case, the deformation of the boundary is exactly prescribed by the global uniform deformation $\tilde{\mathbf{F}}$. Such boundaries are less flexible than the ones that allow fluctuations also on the boundary of the RVE, and, therefore, can be expected to result in a global stiffening of the RVE. This effect decays with distance from the boundary and will be less pronounced for shapes of the RVE with small ratios of boundary affected volume to total volume. This ratio is best for a spherical shape of the RVE and will decrease with its diameter. On the other hand, for plate–like RVEs this effect will be more influential.

Periodic boundary conditions. Spatial periodicity of the displacement fluctuation field $\mathbf{w}(P)$ is equivalent to the existence of three linearly independent constant period vectors $\Delta\mathbf{x}_i \in \mathcal{V}$ such that

$$\mathbf{w}(\mathbf{x}(P)) = \mathbf{w}(\mathbf{x}(P) + \Delta\mathbf{x}_i) \qquad i = 1, 2, 3 \tag{29}$$

holds. For any region $\mathcal{G} \subseteq \mathcal{B}$ with $\kappa(\mathcal{G})$ containing exactly one period in each direction, $\Delta\mathbf{x}_i$, the boundary displacement fluctuation $\mathbf{w}(\partial\mathcal{G})$ is periodic. Equations (27) and (28) hold with the integrals taken over $\mathcal{G}$ in the corresponding placements. The simplest possible initial shape of $\kappa_0(\mathcal{G})$ is a cube.

5 Finite Element Implementation

Spatial Discretization. The calculation of the stress response to a given deformation process is done by using a three-dimensional nonlinear finite-element-analysis. The RVE is discretized by constant strain tetrahedral elements. A formulation for finite deformations is found in Oden (1972). Five tetrahedra, one of them with double the volume, can form a cube in two principal ways, which differ by a rotation of 90° around any edge. Both cube types have to be alternated in each spatial dimension in order to ensure compatibility. Therefore, periodic boundary conditions require an even number of cubes in each direction. The minimal number of elements is determined by the demanded accuracy. Taking one element per grain, we obtain the maximum number of different lattice orientations without allowing nonhomogeneous deformations in the grains. On the other hand, a fine discretization of each grain results in prohibitively large systems, if a certain number of grains is required.

As we have boundary conditions for displacement fluctuations, the nodal displacement vectors $\mathbf{u}_K$ are additively decomposed according to the global placement split:

$$\mathbf{u}_K = (\tilde{\mathbf{F}} - \mathbf{I})\mathbf{X}_K + \mathbf{w}_K \tag{30}$$

with the initial position $\mathbf{X}_K$ of node K and the actual nodal fluctuation $\mathbf{w}_K$.

Reduction of the Global System. Homogeneous or periodic boundary conditions can be implemented by appropriately reducing the global system. This is illustrated by a small two-dimensional example in Fig. 1. The square structure is discretized by 16 nodes. For homogeneous boundary conditions, the fluctuations of the border nodes vanish, the four interior nodes remaining free. For periodic boundary conditions, the node fluctuations at the right border are set to the corresponding ones at the left, thus eliminating four free nodes. The same is done for the upper and lower borders, eliminating three more free nodes. Additionally the fluctuation of one node is set to zero in order to suppress rigid body motions in the fluctuations. Thus, the number of free nodes reduces to 8.

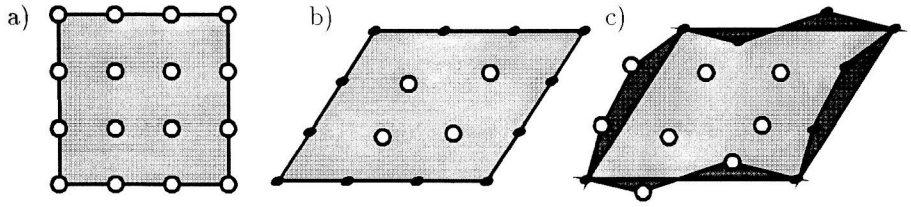

Figure 1. System reduction corresponding to the boundary conditions. a) unreduced system, b) homogeneous boundary conditions, c) periodic boundary conditions (∘ free node, • eliminated node).

The number of structural nodes and elements determines the amount of data to be handled during pre-, main- and postprocessing. The number of elements determines furthermore the computation time needed for evaluating the element routines during assembly of the global stiffness. The bandwidth of the global system for homogeneous boundary conditions depends on the number of nodes per cross section, whereas for periodic boundary conditions it is determined by the number of surface nodes.

Deformation Control. The global deformation process is split into intervals of constant velocity gradient $\tilde{\mathbf{L}} = \dot{\tilde{\mathbf{F}}}\,\tilde{\mathbf{F}}^{-1}$. The actual deformation gradient $\tilde{\mathbf{F}}_t$ is calculated from some intermediate $\tilde{\mathbf{F}}_0$ by

$$\tilde{\mathbf{F}}_t = \exp((t - t_0)\,\tilde{\mathbf{L}})\,\tilde{\mathbf{F}}_0. \tag{31}$$

By this velocity control a constant global strain rate is guaranteed, which is important for the interpretation of rate-dependent material response. Another advantage is the possibility to exactly perform isochoric processes ($\det(\tilde{\mathbf{F}}_t\,\tilde{\mathbf{F}}_0^{-1}) = 1$) by simply taking $\mathrm{tr}(\tilde{\mathbf{L}}) = 0$.

For constant strain elements, the local stresses are constant within the elements. Thus the calculation of the global Cauchy stress reduces to a sum over all elements, weighted by volume.

$$\tilde{\mathbf{T}} = \frac{1}{V}\sum_{e=1}^{\mathrm{NOE}} \mathbf{T}_e\,V_e \qquad V = \sum_{e=1}^{\mathrm{NOE}} V_e \qquad (\mathrm{NOE} = \text{number of elements}). \tag{32}$$

6 Isotropy Tests

Generation of Initial Isotropic State. For studying anisotropies induced by deformations, we need an initially isotropic specimen. This includes isotropy of the elastic stiffness and of the initial yield surface. Roughly speaking, no rigid body rotation shall be detectable by any identification of these parameters.

Principally, such isotropy can be expected for a polycrystalline RVE with random grain growth and a sufficiently high number of grains. For many polycrystalline metals, the grain size is so small in comparison with the size of the structure that these conditions are fulfilled.

In the context of RVE simulations, the selection of suitable initial orientations is a difficult problem, as the number of grains is bounded due to computational limitations.

In literature the following suggestions have been made:

1. Random generation of orientations with homogeneous distribution (Harren and Asaro, 1989; Lipinski, Krier, Berveiller, 1990)
2. Measurement of the orientation in a small region of a real material (Becker, 1991; Lachner, 1995)
3. Generation of regular or quasi-regular sets of orientations

The advantage of the third method is that the number of grains needed to produce isotropy is much smaller than for the other two. This is the reason why we used the third choice which we will describe in more detail.

The selection of a regular set of n orientations out of the set $\mathcal{S}$ of all orientations is non-trivial and remains unsolved for large prescribed numbers. Therefore, iterative numerical algorithms have been constructed to produce at least quasi-regular orientation sets for arbitrary n. They workas follows: First, we choose a continuous metric on $\mathcal{S}$, which is isotropic, i.e. invariant under rotations. There exist infinitely many of such metrics which, however, are all topologically equivalent. Second, we maximize the distances between all orientations of an initially selected set in $\mathcal{S}$. This leads to a non-linear optimization problem which can be iteratively solved by standard procedures (gradient method, simplex method, etc.). The result of such a procedure is a local maximum. In most cases, it is extremely difficult to find and prove global maximality of such a solution, but isotropy tests show us immediately, whether the solution is sufficiently isotropic. It is important for isotropy that the grains assigned to each of these orientations cover the same volume within the RVE. Experience shows that RVEs produced in such a way behave sufficiently isotropic even for a rather small number n.

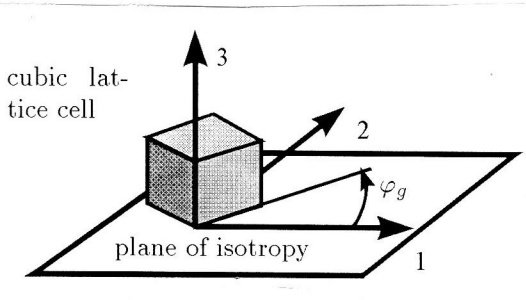

Figure 2. Grain Lattice Position in the Plane of Isotropy

Transverse Isotropy. The complexity of the problem is reduced drastically by limiting the required isotropy to one plane (transverse isotropy). Then a one-dimensional orientation distribution will be sufficient. One lattice direction is fixed to the axis of isotropy (3-axis in Figure 2). Then the lattice for each grain g is determined by an angle φ_g in the plane of isotropy. The construction of an initial orientation distribution becomes rather trivial in this case. The discrete orientations φ_g form classes that cover the total orientation space (e.g. 90° for cubic crystallites). The width of the classes $\Delta\varphi_g$ is set proportional to the grain volume V_g.

$$\frac{\Delta\varphi_g}{V_g} = \frac{90^\circ}{V} \tag{33}$$

For equal grain volumes, the resulting orientation distribution is regular. However, the orientation distribution can be adjusted to any grain volume distribution.

Parameters Tested. The material behaviour has to be evaluated by tests which can be identically performed at different stages of deformation. For the elastic behaviour, we consider the incremental stiffness (ratio of stress increment $\Delta\tilde{\mathbf{T}}$ to strain increment $\Delta t\tilde{\mathbf{D}}$)

$$\Delta\tilde{\mathbf{T}} = \Delta t\, \mathbb{C}_{\text{incr}}[\tilde{\mathbf{D}}] \qquad \text{with} \quad \tilde{\mathbf{D}} = \frac{1}{2}(\tilde{\mathbf{L}} + \tilde{\mathbf{L}}^T) \tag{34}$$

This is valid only for constant velocity gradients $\tilde{\mathbf{L}}$. For a transversly isotropic material, $\mathbb{C}_{\text{incr}}$ should not change when the specimen is rotated in the isotropy plane before the test. Then, any function of $\mathbb{C}_{\text{incr}}$ is a circle in a polar plot over the rotation angle. With test strain rate components

$$[\tilde{\mathbf{D}}] = \begin{bmatrix} \dot{\epsilon} & 0 & 0 \\ 0 & -\dot{\epsilon} & 0 \\ 0 & 0 & 0 \end{bmatrix} \tag{35}$$

the function

$$G = \frac{\Delta \tilde{T}_{11} - \Delta \tilde{T}_{22}}{2G_{\langle 100 \rangle}\, \dot{\epsilon}\, \Delta t} \tag{36}$$

gives in the isotropic case the incremental shear modulus, normalized by the shear modulus $G_{\langle 100 \rangle}$ of the cubic single crystal.

The transverse isotropy of the yield surface is tested in a similar way. In experiments, yielding is detected by different indicators, e.g., by the devitation of the tangent stiffness from the elastic value or by the residual deformation after (supposedly) elastic unloading. In the RVE model, yielding can be detected directly using the physically relevant information about the slip system activity. The ratio of dissipation rate P_{diss} to total stress power P_{tot}

$$d := \frac{P_{\text{diss}}}{P_{\text{tot}}} = \frac{\int_{\mathcal{B}} \sum_\alpha \tau_\alpha \dot{\mu}_\alpha \, \mathrm{d}V}{V \operatorname{tr}(\tilde{\mathbf{T}}\, \tilde{\mathbf{D}})} \tag{37}$$

is taken as a normalized average indicator of yielding.

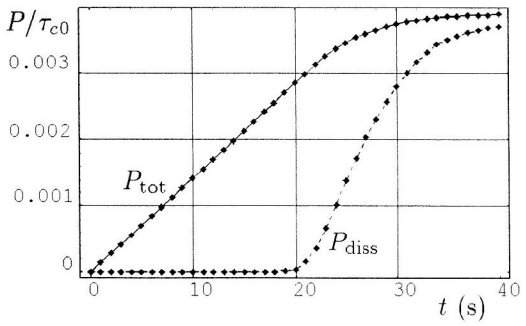

Figure 3. Dissipation Rate and Total Stress Power at the Onset of Yielding

During elastic processes, d is equal to zero. For stationary inelastic processes (constant strain rate, constant stresses), d equals 1. As the material is viscoplastic, the stationary stresses are rate dependent. Fig. 3 shows typical curves of the dissipation rate and the total stress power. As $\tilde{\mathbf{L}}$ is set constant, P_{tot} is proportional to the stresses. The observed smoothness is due not only to the viscosity, but also to the successive activation of slip in differently orientated grains.

For testing isotropy, we compare the v. Mises-stress for $d = 2\%$ and $d = 50\%$. Comparing the results of isotropy tests for deformed and undeformed states, deformation induced elastic and inelastic anisotropy can be detected.

7 Example

RVE Specification. As an example we give some computational results obtained from a RVE with $5 \times 5 \times 5$ nodes and periodic boundary conditions (Figure 4). Although this is a rather small structure (320 tetrahedra, 63 free nodes), it is sufficiently isotropic. Starting from a transverse isotropic stressfree state, we impose a constant velocity gradient until the deformation gradient components reach the values

$$[\tilde{\mathbf{F}}] = \begin{bmatrix} 3/2 & 0 & 0 \\ 0 & 2/3 & 0 \\ 0 & 0 & 1 \end{bmatrix} \tag{38}$$

This means global isochoric plane strain in the plane of transverse isotropy (see Figure 4).

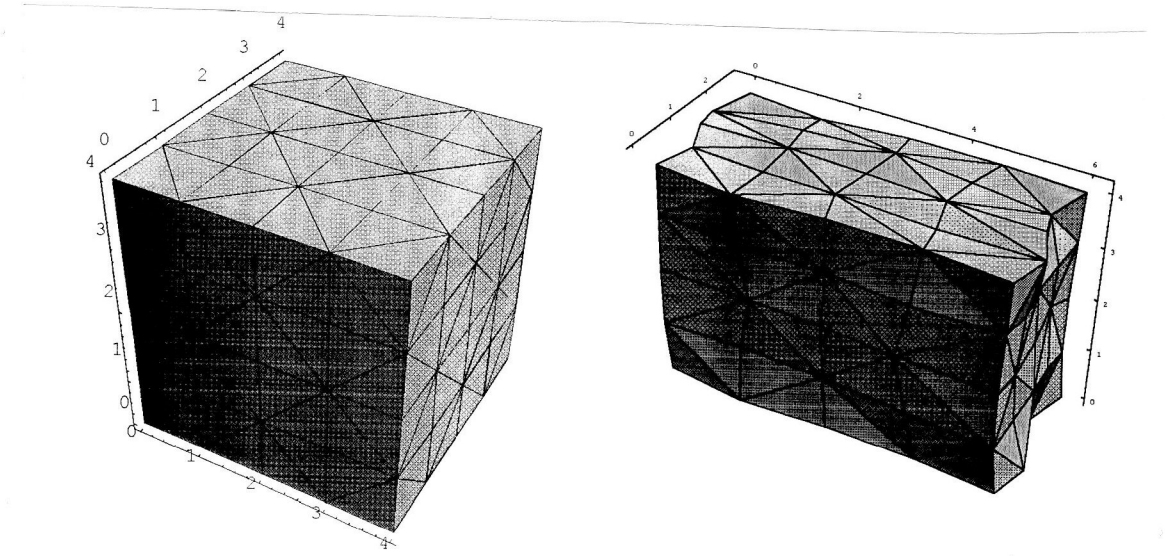

Figure 4. Cubic RVE. Initial State (left), Deformed State (right).

The local constitutive law models face centered cubic single crystals, considering the elastic cubic anisotropy and the octahedral slip systems with equal critical resolved shear stress τ_c. The one-dimensional constitutive law on the slip system level corresponds to a linear viscous and a dry friction element, arranged in parallel (Bingham-body). For separating effects of texture and residual stresses, hardening is not included in this example.

Texture. The texture can be visualized by a density plot of the orientation distribution in the inverse stereographic projection with the 3-direction as pole (Figure 5).

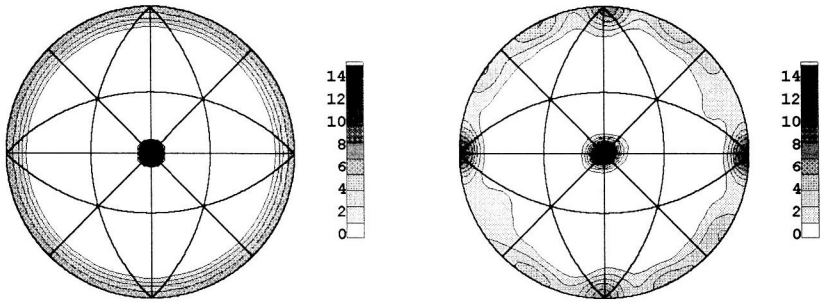

Figure 5. Orientation Distribution. Initial State (left), Deformed State (right).

The density plot of the initial state illustrates the character of the transverse isotropic orientation distribution. All grains have one lattice axis fixed to the isotropy axis (3-direction). They appear as a black point in the centre of the plot. The points corresponding to the other lattice axes are isotropically distributed over the circumference of the plot. For three-dimensional isotropy, the directions should be distributed in a similar way over the surface of the orientation sphere, giving a constant value everywhere in the plot.

In the plot for the deformed state, we observe inhomogeneities along the circumference, in particular a concentration at the four poles. The expansion of the central dark region indicates that the lattice rotation of the grains is partially out of the isotropy (1-2) plane. The orientation distribution is no longer transversly isotropic.

Isotropy Test. The isotropy tests at the deformed state are done after global unloading ($\tilde{\mathbf{T}} = \mathbf{0}$). In order to determine the effect of texture and internal stresses, the isotropy is tested twice, once immediately after global unloading (unloaded state), and, second, after additional relaxation of the internal stresses ($\mathbf{T} = \mathbf{0}$ in all grains). For an isotropy test, a series of simulations with the specimen (RVE) rotated from 0° to 360° and constant spatial velocity gradient have to be performed. For the interpretation of the polar plots, we have to consider that a rotation angle of zero corresponds to a velocity gradient equal to that of the preceding deformation. 90° corresponds to a reversion of the velocity gradient with respect to the material.

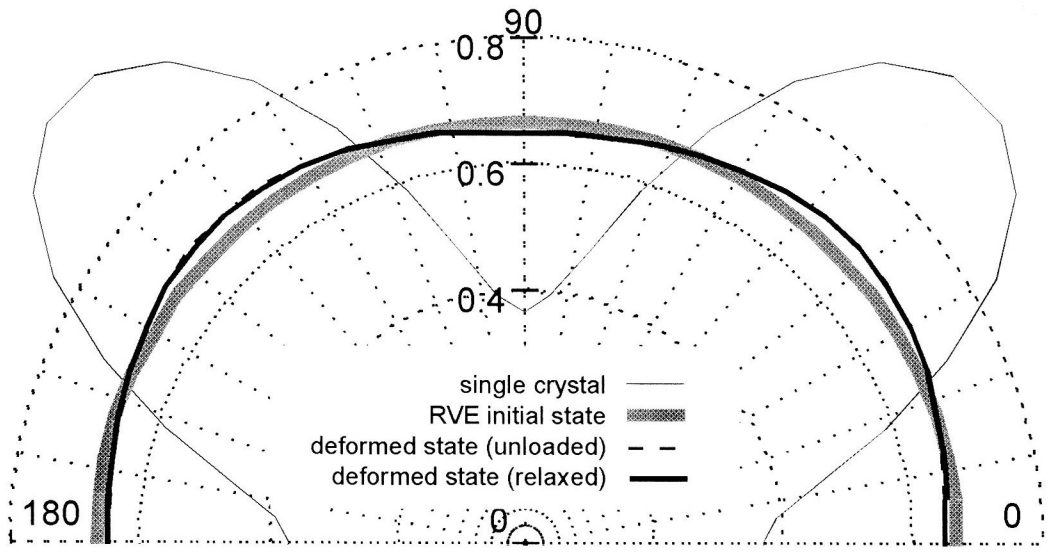

Figure 6. Normalized Shear Modulus G as Function of Rotation Angle α

Elastic Behaviour. In the plot for the normalized shear modulus as defined in equation (36), we observe an induced anisotropy in the elastic behaviour (Figure 6). Deviations of the initial state from isotropy are small (within the plotting accuracy). After the deformation the initial circular curves deform slightly towards the single crystal curve. The existence of internal stresses obviously has no influence on the global elastic behaviour. The corresponding curves nearly coincide.

Inelastic Behaviour. Figure 7 shows the induced anisotropy of the yield surface due to large inelastic deformations. The upper plot indicates the von Mises stress, normalized by the critical resolved shear stress at the onset of yielding ($d = 2\%$), the lower one gives the values for an intermediate state between onset and stationary yielding ($d = 50\%$). Both plots show remarkable sensitivity to internal stresses. For the relaxed state, the anisotropy at both levels of d is similar to that of the elastic behaviour in Figure 6. This can only result from the formation of texture during the deformation. The curves for the unloaded state show that the internal stresses delay the onset of yielding after unloading if the process is continued in the same direction. For loading paths different from the preceding deformation, a considerable loss of yield strength is observed. As this secondary process proceeds, the internal stress distribution changes, and the influence of the primary internal stresses is partially reduced (compare the curves "deformed state (unloaded)" in Figure 7). The redistribution of internal stresses occurs via inelastic deformations comparable in size to the elastic deformations, whereas the texture development is observed only after large inelastic deformations.

8 Conclusions

The representative volume element technique has been presented and discussed. Based on a model for the description of finite inelastic deformations of single crystals, the objective was to simulate the constitutive response of polycrystalline solids including the interaction of neighbouring grains. Some details of a FE simulation were discussed with special attention paid to the boundary conditions. Some features of deformation induced elastic and inelastic anisotropy were shown using a simple computational example. The results illustrate the possibility to identify distinct mechanisms for the development of anisotropy during inelastic deformations, such as residual stresses and lattice rotations (texture development).

Once an RVE has been constructed, we are able to perform any desired simulation on the computer, and to study any mechanism with any precision desired.

The RVE concept turns out to be versatile and promising. It is not restricted to the study of grain interaction, but is open to include the influence of imperfections (voids, inclusions), grain boundary mechanisms, damage, fracture development, and much more.

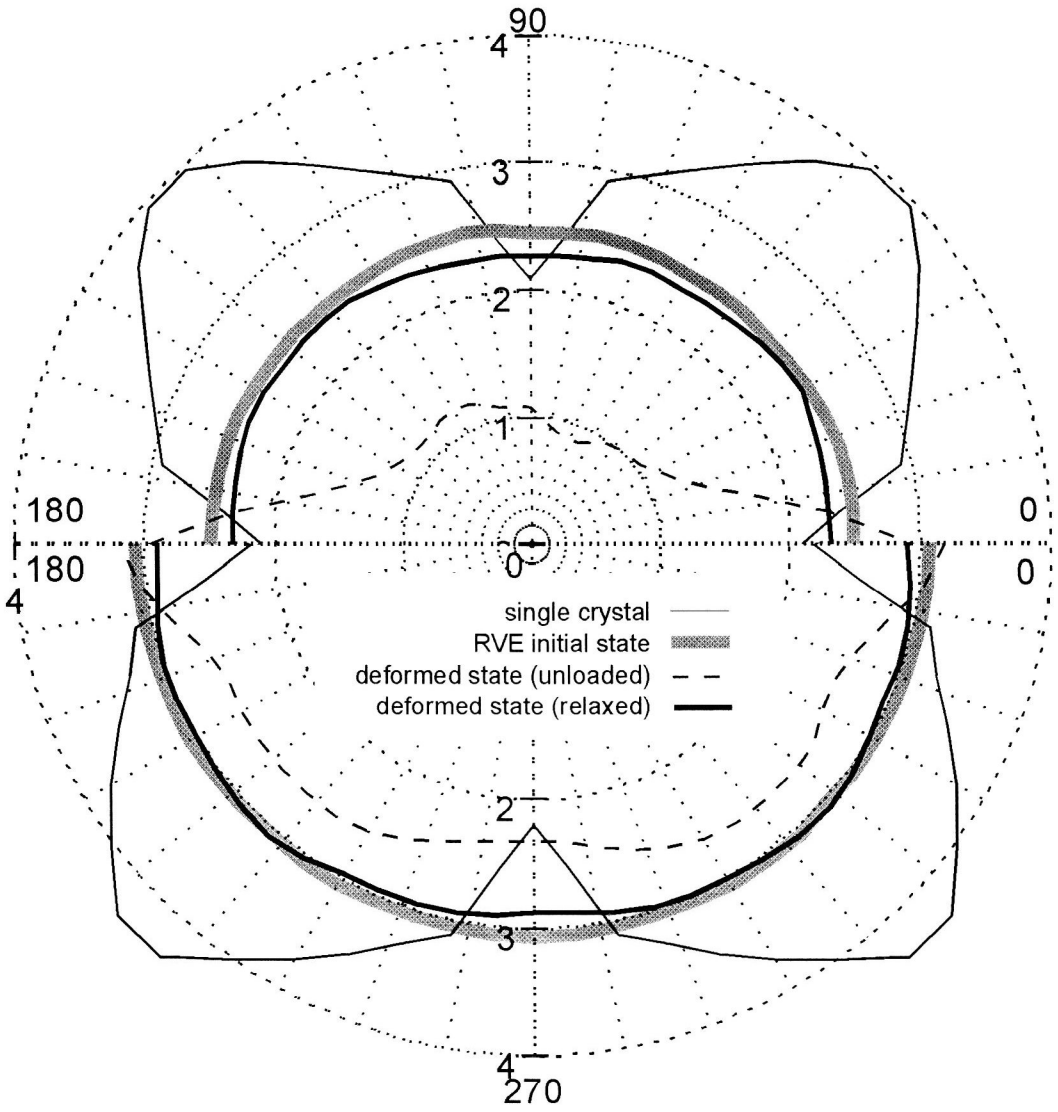

Figure 7. Normalized von Mises stress σ/τ_c at $d = 2\%$ (upper part) and at $d = 50\%$ (lower part) as Function of the Angle of Rotation. As the Curves are Periodical with a Periode of 180°, the Second Half of the Plots have been Omitted.

Literature

1. Becker, R.: Analysis of texture evolution in channel die compression – I. effects of grain interaction, Acta metall. mater, 39, 6, (1991), 1211-1230
2. Bertram, A.: Axiomatische Einführung in die Kontinuumsmechanik, BI Wissenschaftsverlag, Mannheim, (1989)
3. Bertram, A.: Description of Finite Inelastic Deformations, Proceedings of MECAMAT '92 "International Seminar on Multiaxial Plasticity", 1.-4. Sept. 1992 in Cachan, France, Editors: A. Benallal, R. Billardon, D. Marquis, (1992), 821-835
4. Bertram, A.: Beschreibung finiter inelastischer Deformationen mittels materieller Isomorphismen, ZAMM 74, 4, (1994), T314-T316
5. Bertram, A.; Kraska, M.: Beschreibung finiter plastischer Deformationen von Einkristallen mittels materieller Isomorphismen, ZAMM 75, (1995), S179-S180
6. Bertram, A.; Kraska, M.: Description of Finite Plastic Deformations in Single Crystals by Material Isomorphisms, Proceedings of IUTAM & ISIMM Symposium on Anisotropy, Inhomogeneity and Nonlinearity in Solid Mechanics, Editors: D.F. Parker, A.H. England, Kluwer Academic Publ., (1995), 77-90

7. Bertram, A.; Kraska, M.: Determination of Finite Plastic Deformations in Single Crystals, Arch. Mech. 47, 2, (1995), 203-222

8. Han, J.: Identifikation der elastischen Kennwerte anisotroper Hochtemperaturlegierungen mittels Resonanzmessungen und Finite-Elemente-Simulation, Fortschritt-Berichte VDI Reihe 5, Nr. 404, Düsseldorf (1995)

9. Havner, K. S.: Finite Plastic Deformation of Crystalline Solids, Cambridge University Press (1992)

10. Harren, S. V.; Asaro, R. J.: Nonuniform deformations in polycrystals and aspects of the valitidy of the Taylor model, J. Mech. Phys. Solids 37, 2, (1989), 191-232

11. Krawietz, A.: Materialtheorie, Springer Berlin, (1986)

12. Lachner, D.: Plastische Korndrehungen in Metallen – Modelle und Experimente, Fortschr.-Ber. VDI Reihe 5, Nr. 403, Düsseldorf, (1995)

13. Lipinski, P.; Krier, J.; Berveiller, M.: Elastoplasticité des métaux en grandes déformations: comportement global et évolution de la structure interne, Revue Phys. Appl. 25, (1990), 361-388

14. Müller, M.: Plastische Anisotropie polykristalliner Materialien als Folge der Texturentwicklung, Fortschr.-Ber. VDI Reihe 18, Nr 137, Düsseldorf (1993)

15. Noll, W.: A New Mathematical Theory of Simple Materials, Arch. Rat. Mech. Anal. 48, (1972), 1-50

16. Oden, J. T.: Finite Elements of Nonlinear Continua, McGraw-Hill, New York (1972)

17. Schröder, J.; Miehe, C.: Numerische Behandlung von Homogenisierungsprozessen zur Beschreibung von Mikro-Makro-Übergängen, "Große plastische Formänderungen", Bad Honnef 1994, Editor: O. T. Bruhns, Mitteilungen aus dem Institut für Mechanik, Nr.93, Ruhr-Universität Bochum, (1994), 117-120

Addresses: Dipl.-Ing. Martin Kraska, Institut für Mechanik, Technische Universität, Straße des 17. Juni 135, Sekretariat C8, D-10623 Berlin; Professor Albrecht Bertram, Institut für Mechanik, Otto-von-Guericke Universität, Postfach 4120, D-39016 Magdeburg